

Phonon propagation scale and nanoscale order in fused silica from Raman spectroscopy

Vitaly I. Korepanov

Intitute of Microelectronics Technology and High Purity Materials, RAS

In fused silica, the local structure has a crystal-like order at nanometer scale. Raman spectral pattern is sensitive to the phonon confinement length, which makes possible to derive the size information from the spectra. In this work, Raman spectrum of silica is described as localized phonons of SiO₂ network. This allows to estimate the phonon propagation scale, which can be characterized by a distribution over the 0.5-4 nm range.

Introduction

Glasses possess a certain degree of local order as evidenced, in particular, by X-ray diffraction^{1,2} and computational studies³⁻⁷. How to quantify the local order, and how to link the experimental data with understanding of the structure are disputable questions of high interest.

It is argued in the literature that Boson peak in Raman spectra can reflect the nanometer-scale local order⁷⁻¹¹. This broad spectral feature is observed in the low-wavenumber range (LWR) (60-100 cm⁻¹). The bands in Raman spectra of such systems as fused silica and water represent the phonon modes localized by the disorder¹¹⁻¹³. In glasses, the early estimation of the localization length was calculated to be in the order of few interatomic spacings¹⁰.

The coherence range of the continuous network can be estimated from the propagation of phonon-like modes¹⁴. Raman spectral pattern for nanoscale systems is a reflection of this coherence^{8,15}. For the localized (confined) phonons, the Raman spectrum is not limited to the near Brillouin zone (BZ) center modes. The contribution of different k -points depends on the size, and can be found from Fourier decomposition of the confined phonons into the original bulk wavefunctions¹⁵:

$$I(\omega) \cong \iiint \frac{\Gamma_0(\sigma) * |C(\mathbf{q}_0, \mathbf{q})|^2}{(\omega - \omega(\mathbf{q}))^2 + (\Gamma_0(\sigma)/2)^2} d^3\mathbf{q}, \quad (1)$$

where ω is the wavenumber, σ is the confinement size, Γ_0 is the natural linewidth, $C(\mathbf{q}_0, \mathbf{q})$ is the Fourier coefficient for a given confinement shape and size at a given wave vector \mathbf{q} . The scattering intensity at \mathbf{q}_0 depends on the phonon propagation direction, and can be calculated from Raman tensor¹⁶. This gives additional intensity factor $A_i(\mathbf{q}, \varphi, \vartheta)$ for scattering angles φ and ϑ ¹⁷. The intensities should be integrated (numerically) over the scattering directions in polar coordinates and summed up over band index i :

$$I(\omega) \cong \sum_i \iiint \frac{A_i(\mathbf{q}_0, \varphi, \vartheta) * \Gamma_{0,i} * |C(\mathbf{q}_0, \mathbf{q})|^2 * q^2}{(\omega - \omega_i(\mathbf{q}))^2 + (\Gamma_{0,i}(\sigma)/2)^2} d\mathbf{q} d\varphi d\vartheta, \quad (2)$$

Within such approach, the acoustic phonons should have no contribution, because the intensity factors are zero. However, in disordered systems, the Raman intensity for acoustic phonon range is described a different way. It was shown that it has additional wavenumber dependence, referred to as light-to-vibration coupling coefficient $C_{ac}(\omega)$ ¹⁸. Experimental studies

showed that it has a linear wavenumber dependence $C_{ac}(\omega) \sim \omega$ ^{19,20}.

The phonon confinement model formulated in this way was recently applied to hydrogen-bond network of water, it was shown that experimental Raman spectra of liquid water contain highly important information on the size of ice-like structure fragments¹³. The equation (2) links the Raman spectral pattern with the coherence range of the confined phonons. The present study aims at interpretation of the Raman spectra of silica in terms of phonons propagation scale of the SiO₂ network.

Experiment

For the fused silica sample, the high quality UV-transparent microscope slide was taken (Electron Microscopy Sciences). The Raman measurements were carried out at NCTU with a laboratory built spectroscopic system described elsewhere²¹. Excitation wavelength was 532 nm with laser power of 12 mW at the sample point; 20x objective was used. 8 spectra were averaged with acquisition time of 30s. The measured spectra were reduced with the Boltzmann factor and corrected for the ν^3 frequency dependence²¹.

Calculations

Based on the similarities between cristobalite and fused silica glass in terms of structure and Raman spectra^{3,7,22,23}, cristobalite is taken as the structure motif at the nanometer scale for fused silica. The phonon dispersion $\omega(\mathbf{q})$ was calculated with the Quantum Espresso package^{24,25}. The PBEsol functional was taken with high-throughput ultrasoft pseudopotentials²⁶ with cut-off for wavefunctions/charge density of 56/320 Ry. The 12-atom unit cell was taken. The geometry and cell parameters were optimized with 8x8x6 k -point grid; phonon dispersion was calculated with the 8x8x6 grid. Raman tensor was calculated with LDA (PZ) functional with norm-conserving pseudopotentials²⁷ with the cut-off of 112/448 Ry. The intensity factors $A_i(\mathbf{q}, \varphi, \vartheta)$ were calculated from Raman tensor for the vibrational forms for each φ and ϑ . For each band, the intensity factors were scaled according to the experimental spectra of bulk cristobalite. Scaling of the phonon energies was done to match the computed Raman spectral pattern of cristobalite with the experimental data by multiplying the whole dispersion function of the given band $\omega_i(\mathbf{q})$ by the

scaling factor²⁸. The scaling factors were in the range (0.94...1.07).

For the form-factor calculation, spherical confinement was assumed; the Fourier coefficients $C(\mathbf{q}_0, \mathbf{q})$ for this case have an analytic form of Bessel-like function²⁸. The integration in eq. (2) is done within [0,2] range of the reduced wavevector (i.e. not limited to the 1st Brillouin zone²⁹).

The experimental spectra discussed here were corrected by the frequency factor $(\omega - \omega_0)^3$ and Boltzmann distribution factor³⁰. For the correct comparison with the calculated spectra, the latter should also be divided by ω according to the Placzek's expression³¹.

The Raman spectra of the localized phonons were calculated with eq. 2. For the natural linewidth, the inverse size dependence was assumed $\Gamma_i(\sigma) = \Gamma_i(\infty)(1 + g_i/\sigma)$, which reflects the different lifetimes of the localized phonons^{8,32,33}. $\Gamma_i(\infty)$ is the linewidth for the bulk

crystal. $\Gamma_i(\infty)$ and g_i sets of values were determined from experimental data for bulk crystal and fused silica correspondingly.

Results and discussions

For the phonon energies, very good agreement was found of the DFT calculations with the available experimental data and previous calculations⁷. Only minor scaling of the phonon dispersion was required (scaling factors in range 0.94...1.06).

The calculated Raman spectral patterns for different propagation lengths are shown on fig. 1. The bands of the bulk cristobalite broaden asymmetrically upon confinement in accordance with the dispersion functions. The most pronounced size dependence is seen in the low-wavenumber region (LWR).

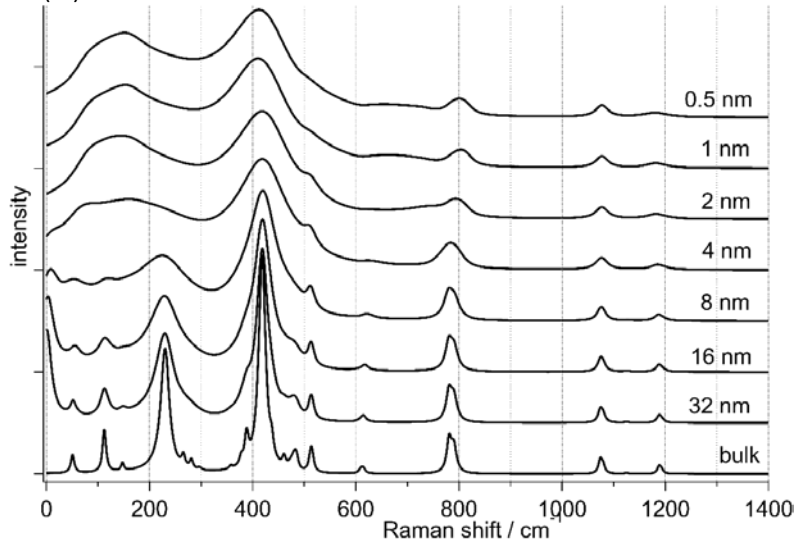


Figure 1. Calculated Raman spectral patterns for different phonon propagation lengths (eq. 2).

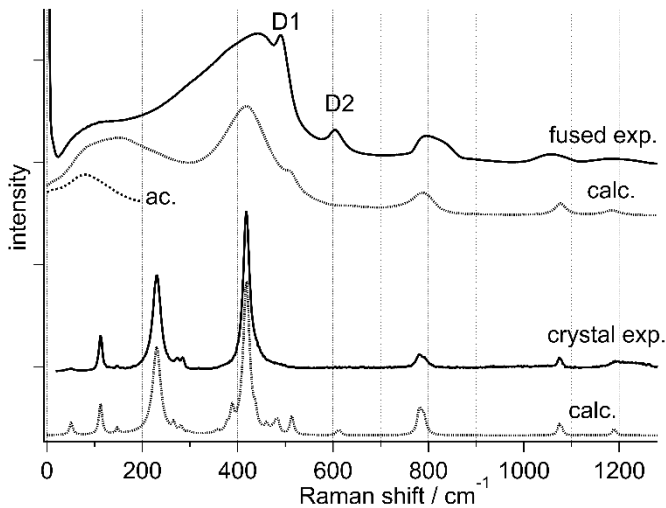


Figure 2. Experimental Raman spectra of fused silica (top, solid line) and cristobalite from ^{22,34} (bottom, solid line); calculated spectra (eq. 2) are shown with dotted lines. For phonon propagation scale in fused silica, the lognormal distribution was considered with mean 1 nm and variance 0.7. The contribution from acoustic modes is plotted separately.

The Raman spectrum of fused silica however is not limited to the vibrations of SiO₂ network (fig. 2). Besides that, the defect bands can be identified, most significant of which are labeled D1 (breathing vibration mode of the 4-member rings) and D2 (breathing vibration mode of the 3-member ring), observed at about 495 and 605 cm⁻¹, respectively^{35,36}.

Comparison of the experimental Raman spectra with calculations allows to estimate the phonon propagation scale. Most pronounced size dependence is found in the low-wavenumber region. If the acoustic phonons are considered separately, the band maximum is highly sensitive to the size in the few-nm range (fig. 3), and arrived to asymptote of ~100 cm⁻¹ for fully-disordered case (sub 1 nm). The LWR band (boson peak) is located in the 60-100 cm⁻¹ range, therefore, most consistent way to describe the coherence length should be a certain distribution of lengths (possibly, log-normal³⁷). For a characteristic spectral pattern, the lognormal size distribution with mean 1 nm and variance 0.7 was considered, which includes significant contribution from the 0.5-4 nm range. This is plotted in fig. 2 in comparison with the spectrum of fused silica.

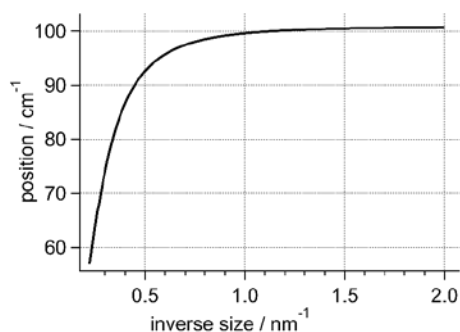


Figure 3. Calculated position of the band maximum for acoustic modes vs. inverse size

Conclusions

In conclusion, the Raman spectral pattern of fused silica can be described as confined phonons of SiO₂ network. Low-wavenumber region of the spectrum has a high sensitivity to the phonon propagation scale. Comparison of experimental and calculated spectral patterns allows to estimate the coherence range of the structure, which can be described as a distribution between 0.5 and 4 nm.

Acknowledgements

Many thanks to Dr. D.M. Sedlovets for providing the computational facility for this work, Chun-Chieh Yu, Ankit Raj and Prof. Hiro-o Hamaguchi (USILab, NCTU) for help with spectral measurements. This work was supported by the Ministry of Science and Higher Education of the Russian Federation, program no. 075-00475-19-00.

References

- 1 R. K. Biswas, P. Khan, S. Mukherjee, A. K. Mukhopadhyay, J. Ghosh and K. Muraleedharan, Study of short range structure of amorphous Silica from PDF using Ag radiation in laboratory XRD system, RAMAN and NEXAFS, *J. Non. Cryst. Solids*, 2018, **488**, 1–9.
- 2 L. Cartz, An x-ray diffraction study of the structure of silica glass, *Zeitschrift für Krist. - Cryst. Mater.*, 1964, **120**, 241–260.
- 3 M. Lazzeri and F. Mauri, First-Principles Calculation of Vibrational Raman Spectra in Large Systems: Signature of Small Rings in Crystalline SiO₂, *Phys. Rev. Lett.*, 2003, **90**, 036401.
- 4 H. Niu, P. M. Piaggi, M. Invernizzi and M. Parrinello, Molecular dynamics simulations of liquid silica crystallization., *Proc. Natl. Acad. Sci. U. S. A.*, 2018, **115**, 5348–5352.
- 5 P. Umari, X. Gonze and A. Pasquarello, Concentration of Small Ring Structures in Vitreous Silica from a First-Principles Analysis of the Raman Spectrum, *Phys. Rev. Lett.*, 2003, **90**, 027401.
- 6 P. Umari and A. Pasquarello, Infrared and Raman spectra of disordered materials from first principles, *Diam. Relat. Mater.*, 2005, **14**, 1255–1261.
- 7 B. Wehinger, A. Bosak, K. Refson, A. Mirone, A. Chumakov and M. Krisch, Lattice dynamics of α -cristobalite and the Boson peak in silica glass, *J. Phys. Condens. Matter*, 2015, **27**, 305401.
- 8 G. Gouadec and P. Colomban, Raman Spectroscopy of nanomaterials: How spectra relate to disorder, particle size and mechanical properties, *Prog. Cryst. Growth Charact. Mater.*, 2007, **53**, 1–56.
- 9 N. Zotov, I. Ebbsjö, D. Timpel and H. Keppler, Calculation of Raman spectra and vibrational properties of silicate glasses: Comparison between Na₂Si₄O₉ and SiO₂ glasses, *Phys. Rev. B - Condens. Matter Mater. Phys.*, 1999, **60**, 6383–6397.
- 10 T. Nakayama, Strongly localized modes as the origin of the Bose peak in glasses, *Phys. B Condens. Matter*, 1999, **263**, 243–247.
- 11 S. N. Taraskin and S. R. Elliott, Phonons in vitreous silica: Dispersion and localization, *Europhys. Lett.*, 1997, **39**, 37–42.
- 12 M. Montagna, G. Vilianni and E. Duval, Models of Low-Wavenumber Raman Scattering from Glasses, *J. Raman Spectrosc.*, 1996, **27**, 707–713.
- 13 V. I. Korepanov and H. Hamaguchi, Ordered structures in liquid water as studied by Raman spectroscopy and the phonon confinement model, *Bull. Chem. Soc. Jpn.*, 2019, accepted, doi: 10.1246/bcsj.20190044.
- 14 D. C. Elton and M. Fernández-Serra, The hydrogen-bond network of water supports propagating optical phonon-like modes, *Nat. Commun.*, 2016, **7**, 10193.
- 15 H. Richter, Z. P. Wang and L. Ley, The one phonon Raman spectrum in microcrystalline silicon, *Solid State Commun.*, 1981, **39**, 625–629.
- 16 N. S. Shcheblanov, M. E. Povarnitsyn, K. N. Mishchik and A. Tanguy, Raman spectroscopy of femtosecond multipulse irradiation of vitreous silica: Experiment and simulation, *Phys. Rev. B*, 2018, **97**, 1–8.
- 17 V. I. Korepanov, S.-Y. Chan, H.-C. Hsu and H. Hamaguchi, Phonon confinement and size effect in Raman spectra of ZnO nanoparticles, *Heliyon*, 2019, **5**, e01222.
- 18 R. Shuker and R. Gammon, Raman-Scattering Selection-Rule Breaking and the Density of States in Amorphous Materials, *Phys. Rev. Lett.*, 1970, **25**, 222–225.
- 19 M. Zanatta, G. Baldi, S. Caponi, A. Fontana, E. Gilioli, M. Krish, C. Masciovecchio, G. Monaco, L. Orsingher, F. Rossi, G. Ruocco and R. Verbeni, Elastic properties of permanently densified silica: A Raman, Brillouin light, and x-ray scattering study, *Phys. Rev. B*, 2010, **81**, 212201.
- 20 S. Caponi, S. Corezzi, D. Fioretto, A. Fontana, G. Monaco and F. Rossi, Effect of polymerization on the boson peak, from liquid to glass, *J. Non. Cryst. Solids*, 2011, **357**, 530–533.
- 21 H. Okajima and H. Hamaguchi, Accurate intensity calibration for low wavenumber (–150 to 150 cm⁻¹) Raman spectroscopy using the pure rotational spectrum of N₂, *J. Raman Spectrosc.*, 2015, **46**, 1140–1144.
- 22 V. . Sigaev, E. . Smelyanskaya, V. . Plotnichenko, V. . Koltashev, A. . Volkov and P. Pernice, Low-frequency band at 50 cm⁻¹ in the Raman spectrum of cristobalite: identification

- of similar structural motifs in glasses and crystals of similar composition, *J. Non. Cryst. Solids*, 1999, **248**, 141–146.
- 23 S. Malo, O. Pérez and M. Hervieu, Spherulite-shaped cristobalite by fused silica devitrification, *J. Cryst. Growth*, 2011, **324**, 268–273.
- 24 P. Giannozzi, S. Baroni, N. Bonini, M. Calandra, R. Car, C. Cavazzoni, D. Ceresoli, G. L. Chiarotti, M. Cococcioni, I. Dabo, A. Dal Corso, S. de Gironcoli, S. Fabris, G. Fratesi, R. Gebauer, U. Gerstmann, C. Gougoussis, A. Kokalj, M. Lazzeri, L. Martin-Samos, N. Marzari, F. Mauri, R. Mazzarello, S. Paolini, A. Pasquarello, L. Paulatto, C. Sbraccia, S. Scandolo, G. Sclauzero, A. P. Seitsonen, A. Smogunov, P. Umari and R. M. Wentzcovitch, QUANTUM ESPRESSO: a modular and open-source software project for quantum simulations of materials., *J. Phys. Condens. Matter*, 2009, **21**, 395502.
- 25 P. Giannozzi, O. Andreussi, T. Brumme, O. Bunau, M. Buongiorno Nardelli, M. Calandra, R. Car, C. Cavazzoni, D. Ceresoli, M. Cococcioni, N. Colonna, I. Carnimeo, A. Dal Corso, S. de Gironcoli, P. Delugas, R. A. DiStasio, A. Ferretti, A. Floris, G. Fratesi, G. Fugallo, R. Gebauer, U. Gerstmann, F. Giustino, T. Gorni, J. Jia, M. Kawamura, H.-Y. Ko, A. Kokalj, E. Küçükbenli, M. Lazzeri, M. Marsili, N. Marzari, F. Mauri, N. L. Nguyen, H.-V. Nguyen, A. Otero-de-la-Roza, L. Paulatto, S. Poncé, D. Rocca, R. Sabatini, B. Santra, M. Schlipf, A. P. Seitsonen, A. Smogunov, I. Timrov, T. Thonhauser, P. Umari, N. Vast, X. Wu and S. Baroni, Advanced capabilities for materials modelling with Quantum ESPRESSO, *J. Phys. Condens. Matter*, 2017, **29**, 465901.
- 26 K. F. Garrity, J. W. Bennett, K. M. Rabe and D. Vanderbilt, Pseudopotentials for high-throughput DFT calculations, *Comput. Mater. Sci.*, 2014, **81**, 446–452.
- 27 M. J. van Setten, M. Giantomassi, E. Bousquet, M. J. Verstraete, D. R. Hamann, X. Gonze and G. M. Rignanese, The PSEUDODOJO: Training and grading a 85 element optimized norm-conserving pseudopotential table, *Comput. Phys. Commun.*, 2018, **226**, 39–54.
- 28 V. I. Korepanov and H. Hamaguchi, Quantum-chemical perspective of nanoscale Raman spectroscopy with the three-dimensional phonon confinement model, *J. Raman Spectrosc.*, 2017, **48**, 842–846.
- 29 K. Roodenko, I. Goldthorpe, P. McIntyre and Y. Chabal, Modified phonon confinement model for Raman spectroscopy of nanostructured materials, *Phys. Rev. B*, 2010, **82**, 115210.
- 30 H. Okajima, M. Ando and H. Hamaguchi, Formation of “Nano-Ice” and Density Maximum Anomaly of Water, *Bull. Chem. Soc. Jpn.*, 2018, bcsj.20180052.
- 31 A. Calzolari and M. B. Nardelli, Dielectric properties and Raman spectra of ZnO from a first principles finite-differences/finite-fields approach, *Sci. Rep.*, 2013, **3**, 2999.
- 32 S. Kelly, F. H. Pollak and M. Tomkiewicz, Raman Spectroscopy as a Morphological Probe for TiO₂ Aerogels, *J. Phys. Chem. B*, 1997, **101**, 2730–2734.
- 33 A. Pottier, S. Cassaignon, C. Chanéac, F. Villain, E. Tronc and J.-P. Jolivet, Size tailoring of TiO₂ anatase nanoparticles in aqueous medium and synthesis of nanocomposites. Characterization by Raman spectroscopy, *J. Mater. Chem.*, 2003, **13**, 877–882.
- 34 B. Lafuente, R. T. Downs, H. Yang and N. Stone, in *Highlights in Mineralogical Crystallography*, DE GRUYTER, Berlin, München, Boston, 2016, pp. 1–30.
- 35 A. Alessi, S. Agnello, G. Buscarino and F. M. Gelardi, Raman and IR investigation of silica nanoparticles structure, *J. Non. Cryst. Solids*, 2013, **362**, 20–24.
- 36 F. L. Galeener and A. E. Geissberger, Vibrational dynamics in ³⁰Si-substituted vitreous SiO₂, *Phys. Rev. B*, 1983, **27**, 6199–6204.
- 37 R. B. Bergmann and A. Bill, On the origin of logarithmic-normal distributions: An analytical derivation, and its application to nucleation and growth processes, *J. Cryst. Growth*, 2008, **310**, 3135–3138.